

Chapter II

2 Experimental Techniques

Coating the substrate with a barrier coating or a cathodic coating finds an extensive application for the corrosion prevention as discussed in chapter I. The need for protective coating in both industrial sector and commercial is ever growing, it ranges from automobile body panels to discrete parts like fasteners, brackets and various components used in the engine compartment. High-speed cutting tools and other machining tools with high hardness are not an exemption. In view of this ever-growing need for these protective coatings, the present work is designed to study the deposition of zinc-nickel alloy, zinc-cobalt alloy and multi element metal oxide coating, former two coatings were done by electrodeposition and last mixed oxide coating is done by spray pyrolysis technique.

This chapter introduces to the various techniques of sample preparation and the various instrumental analyses done for characterizing the coatings thus obtained. The basic principles, the means and the merits of the techniques are emphasized along with the methods of the preparation of the samples used in the present work.

2.1 Substrate cleaning

Plating of the zinc-nickel alloy was done on commercial mild steel panels of dimensions 4X5 cm. Before plating the panels were cleaned by the following sequences of operation given by Abibsi et.al. [37].

The panels were anodically degreased in a commercial alkaline solution at $4 A/dm^2$ and $60^\circ C$ for 60 seconds, then rinsed in cold distilled water. They were then dipped in hydrochloric acid (50%) and then rinsed in cold distilled water. This was followed by a cleaning step using commercial cyanide solution at $4 A/dm^2$ for 60 seconds and then rinsed in cold distilled water. They were then dipped in sulfuric acid (20%) and then rinsed in cold distilled water. Cleaned specimens were stored in a desiccator.

2.1.1 Zinc-Nickel codeposition

Though pure zinc coating is widely used for corrosion protection, inclusion of small amount of alloying element such as nickel would increase the corrosion resistance greatly. It has been determined by Abibsi et.al. [35,36] that the acetic acid salt spray and electrochemical tests optimum performance is obtained when the concentration of the nickel in the coating is around 12% [37]. Though there are various bath formulations available commercially for e.g. chloride [38], sulfate [39],

sulfate-sulfamate [40], sulfate-chloride [41], pyrophosphate [42], acid chloride based plating bath developed by Abibsi et.al.[37] was followed for this work. Basic composition of the plating solution and the experimental set up is as follows:

Plating bath composition

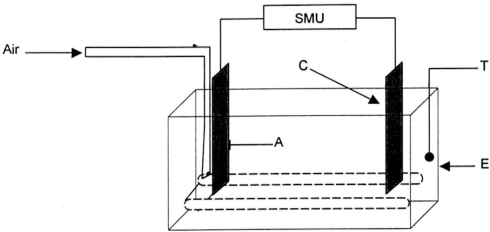
The plating solution had a base composition of $ZnCl_2$ (62.5 g/l) giving a zinc metal concentration of 30 g/l, ammonium chloride (200.0 g/l) and ammonia (25%, 50.0 ml/l). The nickel concentration in the bath was maintained around 5 to 10 g/l of nickel metal concentration. The pH of the solution was adjusted to 5.5 by addition of small amounts of hydrochloric (50%) acid or ammonia (25%). Temperature of the bath was maintained at $30.0 \pm 0.5^\circ C$. Pure zinc plates were used as the anode. Chemicals used were of reagent grade and obtained from Fluka chemicals.

Electroplating

Electroplating of zinc-nickel codeposit was done on the mild steel specimens cleaned by the above said process. The electroplating cell was a 1500-ml bath equipped with three electrodes. The cathode was a 4X5 cm mild steel plate centered between two anodes of pure zinc of the same size. Air inlet tubes were provided to facilitate air agitation.

Abibsi et.al [37]. had already done an elaborate work on the influence of various bath parameters on the coating characteristics, including the effect of agitation. They had proved that effect of agitation results in high concentration of nickel when compared with the one without agitation. In this present work two set of experiments were performed one with air agitation and other under sonication using Bandelin Sonorex Rk100- (35kHz). Sonication is looked into as an alternative way to agitate expecting changes in surface morphology and the composition of the deposit. Keeping the bath composition the same, the current density was varied from $1A/dm^2$ to $5A/dm^2$ for both air-agitated and sonicated deposition. These constant current were supplied to the electroplating cell with the aid of KEITHLEY High Voltage Source Measuring Unit (model 237) which is capable of supplying constant current and measure the voltage simultaneously of any system. Figure 2.1 and 2.2 shows schematic of the setup used for depositing the alloys under air agitation and sonication respectively.

2.1.2



- SMU : Source Measure Unit (constant Current Source)
- A : Anode (Zinc)
- C : Cathode (Mild Steel)
- E : Electroplating bath
- T : Temperature controller

Figure 2.1 Schematic of the electrodeposition unit used in depositing zinc nickel alloy and zinc-cobalt alloy under air-agitated condition

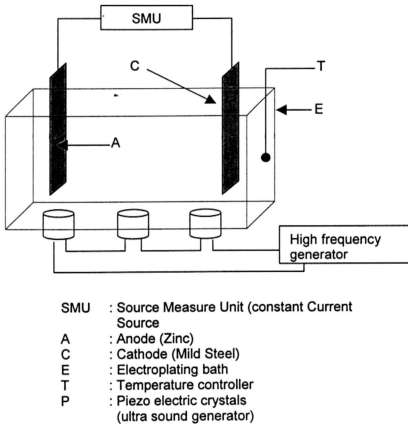


Figure 2.2 Schematic of the electrodeposition unit used in depositing zinc nickel alloy and zinc-cobalt alloy under sonicated condition

Zinc-Cobalt Deposition

The substrates were cleaned as said in section 2.1. The plating bath, which was used to deposit Zinc-Cobalt alloy, contains 78 gm/l of $ZnCl_2$, 16.15 gm/l of $CoCl_2 \cdot 6H_2O$, 200 gm/l of NaCl and 20 gm/l of H_3BO_3 . Electroplating was done in a cell similar to the one used for deposition of Zinc-Nickel alloy. The deposition was carried out under various plating current densities ranging from 1 A/dm² to 5 A/dm². Like Zinc-Nickel deposition, Zinc-Cobalt deposition was also carried out under two modes of agitation, air agitation and sonication.

2.2 Spray pyrolysis

Metal chlorides undergo hydrolysis at elevated temperatures. This is a highly endothermic reaction requiring very high temperature and also reversible. This is done by spraying a fine mist of the metal chloride salt solution (in an organic solvent and water mixture) into a furnace at high temperature. During the process of travelling, the metal chloride reacts with water molecules under go hydrolysis which inturn get oxidized to form metal oxides [43,44]. This technique is called Spray Pyrolysis as it involves spraying the reactants into a furnace and then pyrolysing the reactants. This method has been used to form several structurally important materials like SnO_2 , ITO [11], TiO_2 [45]. The basic steps

involved in depositing a thin film by this method involve the steps as shown in figure 2.3

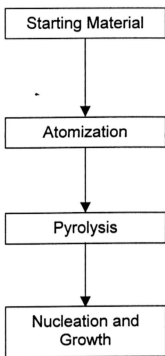


Figure 2.3 Basic Steps in thin film deposition by spray pyrolysis

To ensure that pyrolysis will take place only directly in front of the substrate surface, it is necessary to keep the temperature of the initial material below the decomposition temperature. This is achieved by dissolving the substance in a solvent, atomizing and carrying the fine droplets to the hot substrate with the carrier gas. The major advantage of this technique is the ability to control the particle size with ease, also it is possible to get various coating in different stoichiometry by varying the composition of the feed directly. In figure 2.4 the changes in deposition

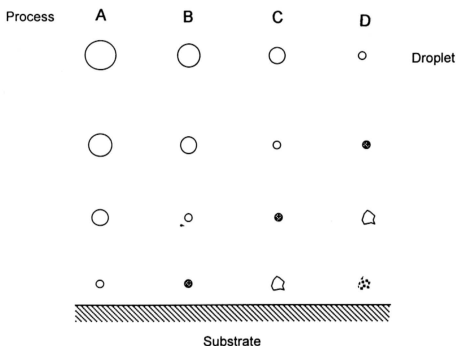


Figure 2.4 Illustration of the various deposition processes involved in relation to the droplet size, in spray pyrolysis.

process with varying droplet size is shown. If the droplet is large (process A in figure 2.4) that the heat absorbed from the surroundings will not be sufficient to vaporize the solvent on the way to the substrate. The droplet hits the surface, where the solvent is completely vaporized leaving a dry, loose precipitate of the starting material. Owing to the reduction in droplet size in process B, the solvent vaporizes completely before it reaches the substrate and then hits the substrate in a statistical distribution. Process C includes the classical chemical vapor deposition process leading to optimum film properties. In this process is entirely vaporized short of the substrate. Before the particle reaches the substrate, there is sufficient time for it to warm up to the ambient

temperature. The particle then melts and vaporizes and undergoes a heterogeneous reaction. This reaction is divided into the following steps.

- a) Diffusion of the reactant molecules to the surface
- b) Adsorption of one or several reaction molecule to the surface
- c) Surface diffusion, chemical reaction, incorporation into the lattice,
- d) Desorption of product molecules from the surface, and
- e) Diffusion of product molecules away from the surface into vapor space.

In process D due to the reduction in droplet size the solvent vaporizes completely while it is far away from the substrate. The particle melts and vaporizes and a chemical reaction will occur in vapor phase. This is a homogenous reaction and because all reactants condense as microcrystallites, they form a powdery precipitate on the substrate. In order to achieve maximum efficiency, most of the droplets must undergo the process described in C and optimization of all the deposition parameters becomes necessary.

2.2.1 Experimental setup

This technique utilizes a custom designed ceramic furnace, and an atomizer. Figure 2.5 shows the schematic of the experimental setup.

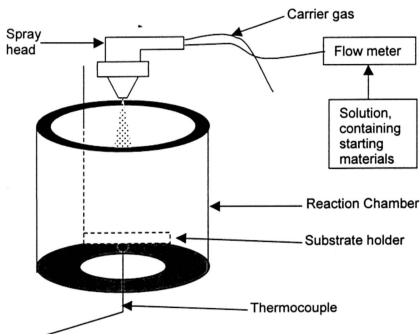


Figure 2.5 Schematic of the experimental setup used in this work for coating thin films of multi element metal oxide.

A furnace of 0.15-m diameter and 0.35-m in height was fabricated and used as the reaction chamber. The furnace can reach up to a maximum of 900°C along a uniform zone of 0.15-m. The furnace was designed to have opening at the both the ends, so that the effluent gases can leave the reaction chamber ensuring the environment inside

chamber to be clean without the effluents. A stainless steel plate with a holder, which acts as a substrate holder, was placed in the chamber and a thermocouple (chromel-alumel) was placed touching the bottom of the substrate holder so as to measure the temperature of the substrate.

A spray gun (Model: KP-7s-12) was used for generating the droplets. The droplet size can be varied by adjusting the needle valve (to adjust the flow of liquid) and the air regulator. A detailed sketch of the spray gun is shown in figure 2.5A. Before the inlet of the liquid a flow meter with valve was attached to measure and control the flow of the liquid. Nitrogen gas of 99% purity was used as the carrier gas through out the experiment. The spraying solution consists of $Zn(NO_3)_2$ and $FeCl_3$ in equi-molar as a 10% solution in isopropyl alcohol. After the required temperature is reached, the substrate was introduced prior and the chamber was flushed with nitrogen gas to remove air from the chamber which other wise could oxidize the mild steel substrate. Purging of nitrogen was continued until the substrate comes into thermal equilibrium with the ambient and then sprayed with the solution, the temperature of the substrate was monitored simultaneously so that the temperature did not drop down below $2^\circ C$ of the processing temperature. After attaining the required thickness the spraying and the heating of the furnace were stopped (few trials were made to get an adequate thickness of $4-6\mu m$ and the measured time or number of spray pulses used). The substrates were then removed after the system cools down to $100^\circ C$. The coatings

thus obtained were characterized using SEM, X-ray diffraction and impedance analysis and the results were presented in chapter 5.

No.	PARTS
1	body
2	cap
3	nozzle
4	cap band
5	nut
5-1	packing
5-2	needle pipe
5-3	needle ring
6	needle valve
7	needle socket
8	needle cylinder
9	air valve set
9-1	rubber packing
9-2	air valve
9-3	valve axle
9-4	valve spring
9-5	nut
10	screw
11	lever
12	regulator
13	air regulator set
13-1	valve
13-2	spring
13-3	O-ring
13-4	air regulator
13-5	screw
14	spreader set
14-1	O-ring
14-2	regulator
14-3	screw
14-4	axle
14-5	pin
15	air nipple
16	spring
17	screw
18	nipple

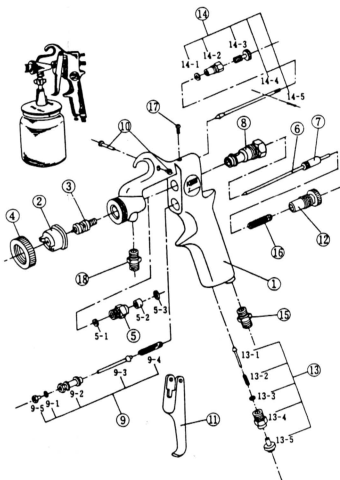


Figure 2.5A Exploded view of the spray gun used in the experiment to spray the precursor into the reaction chamber as fine droplets.

2.3 Analytical Tools

The coatings obtained by the above-described methods are then analyzed for their crystallographic nature, composition, surface morphology and corrosion property by the following instruments or techniques.

2.3.1 X-ray Diffraction

X-ray diffraction is a versatile, non-destructive analytical technique for identification and quantitative determination of the various crystalline forms, known as 'phases', of compounds present in solid materials and powders. The phenomenon of diffraction occurs when penetrating radiation, such as X-rays, enters a crystalline substance and is scattered. The direction and intensity of the scattered (diffracted) beams depend on the orientation of the crystal lattice with respect to the incident beam. A crystal lattice is a regular three-dimensional distribution (cubic, rhombic, etc.) of atoms in space. These crystals are arranged so that they form a series of parallel planes separated from one another by a distance 'd', which varies according to the nature of the material. For any crystal, planes exist in a number of different orientations - each with its own specific d-spacing.

When a monochromatic x-ray beam with wavelength λ is projected onto a crystalline material at an angle θ , diffraction occurs only when the

distance traveled by the rays reflected from successive planes differs by a complete number n of wavelengths. The relation between the θ and ' n ' is given by Bragg's law:

$$n\lambda = 2d \sin \theta$$

By varying the angle θ , the Bragg's Law conditions are satisfied by different d -spacings in polycrystalline materials. Plotting the angular positions and intensities of the resultant diffracted peaks of radiation produces a pattern which is characteristic of the sample. Where a mixture of different phases is present, the resultant diffractogram is formed by addition of the individual patterns. The diffractometer in the present study (Philips PW 1840) utilizes a sample holder, a goniometer, and a fixed-position detector to measure the diffraction patterns of unknowns. The goniometer provides a wide range of angle of incidence, and the detector measures the intensity of the diffracted beam. The resulting analysis is described graphically as a set of peaks with intensity in counts per second (cps) on the Y-axis and goniometer angle (2θ) on the X-axis. Figure 2.6 shows the schematic sketch of a typical X-ray diffractometer.

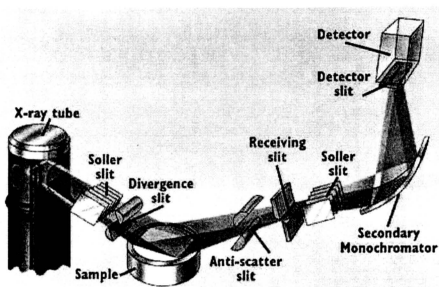


Figure 2.6 Schematic of a typical X-ray diffractometer used in the experimental studies related to the structural analysis.

2.3.2 Scanning Electron Microscope (SEM)

SEM was carried out with Philips 515 scanning electron microscope. Since its invention in the early sixties, SEM has been utilized in many surface science studies. An electron microscope is an electron accelerator that focuses the electron beam with the aid of electromagnetic lenses. The accelerating voltage is typically in the range of 60-100 keV. The illumination source is a tungsten filament, also known as the electron gun, which is enclosed in a metal cylinder called Wehnelt cylinder or cathode and heated to a high temperature (2700°K) causing electrons to be released from the tip of the filament. Lenses focus the electron beam and magnify the image after the electrons pass through

the specimen. The lenses and the specimen stage are mounted in a vertical, lead-lined cylindrical column that allows the interior to be maintained under vacuum. The vacuum is needed so that the electrons do not collide with air molecules and get knocked off course before they reach the specimen. A good vacuum is required (10^{-7} torr) since the mean free path of an electron is 125 cm in a vacuum of 10^{-4} torr. In the *scanning electron microscope* (SEM), a beam of accelerated electrons is used to image surface features of specimens. The surface topography of a specimen is generated by the electrons reflected (back scattered) or given off (secondary electrons) by a metal-coated (gold or gold-palladium) specimen struck by the electron beam. This is accomplished by focusing a narrow, intense beam of electrons to form a very small spot of illumination (between 2Å & 200Å diameter) on the specimen. This fine spot is then moved sideways by deflecting the beam so that a very narrow ribbon of specimen, whose width corresponds to the diameter of the spot, is traversed by the electron probe spot. The probe spot is then returned very rapidly to a point on the specimen one spot diameter above or below the original starting point, and the adjacent ribbon of specimen is then traversed. The process is repeated until the whole area of the specimen has been covered by this "scanning" probe spot of electrons. The pattern of lines is called a raster, and is just like the ones seen on the screen of a television set. A visual image corresponding to the signal produced by the interaction between the beam spot and the specimen at

each point along each scan line is simultaneously built up on the face of a cathode ray tube (CRT) in the same way as a television picture is generated. The specimen image then appears in a similar way to the pictures seen on a black & white television screen. Following Figures 2.7 and 2.8 gives the cross section of the electron gun in SEM and the layout of scanning electron microscope[47].

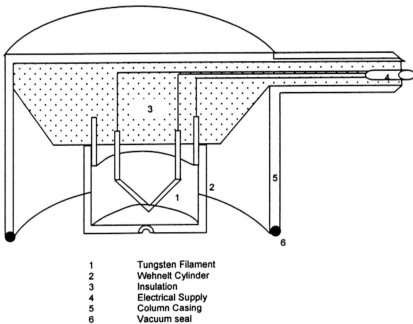
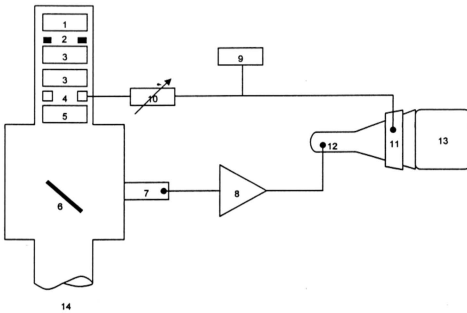


Figure 2.7 Cross-section of an electron gun in SEM



Electron Optical Column

Display/electronics

1. Electron Gun
2. Anode disc
3. Condenser lens
4. Scan coils
5. Objective lens
6. Specimen
7. Detector

8. Signal amplifier
9. Waveform generator
10. Magnification coil
11. Scan coils
12. CRT brightness control
13. CRT display screen
14. Vacuum connection

Figure 2.8 Schematic of a Scanning electron Microscope

2.3.3 Energy Dispersive X-ray Analysis

LEICA S440 scanning electron microscope coupled with EDAX accessory was used to analyze the chemical composition of the sample surface. X-ray microanalysis can be considered as a quantitative and non destructive techniques that allows *in situ* detection of elements as low as 10^{-19} g. Its limitations are that it cannot distinguish between ionic, non-ionic and isotopic species and EDAX in particular cannot detect the low atomic number elements. EDAX fitted with Beryllium window detectors can detect elements with $Z > 11$ while windowless detectors can detect elements with $Z > 5$. In an atom the orbiting electrons are arranged in distinct energy bands or shells. These bands and shells are designated as K, L, M, N, etc. The electrons in the inner most shell i.e. K shell need more energy than the other shells. If an electron knocks one of the K shell electrons a vacancy is created, since the vacancy is created at higher energy, an electron from an outer shell, L, M, N, etc can fill in this vacancy restoring the atom to the ground state or non-excited state. An amount of energy equal to the difference in energy between the shells involved in the transition will be released as photons. If the ejected electron was from an inner shell (K, L, M) then the energy is such that the photon is an X-ray. Although the shells have distinct energies, within these shells the energy of the electrons differs with the atomic number.

This is because of the dependency of the positive charge of the nucleus on the atomic number. Even between elements of adjacent atomic number this variation is significant. Hence whenever an electron transition occurs, the energy released is characteristic for each atomic number and therefore characteristic to each element.

In the present study, EDAX was used to determine the composition of the electrodeposited alloy coatings and the oxide coating obtained by spray pyrolysis, where the principle elements under investigations were zinc, nickel and cobalt, iron and oxygen. The samples were mounted on an aluminum stub using conductive carbon adhesive tape so as to establish good electrical contact between the sample and the holder. For consistency of results, not at least five different locations were analyzed accumulating more than 370,000 counts (total spectrum) for 100 seconds as live time. The elemental concentration were calculated by the built in software and represented in both atomic percentage and weight percentage.

2.3.4 Scanning tunneling microscopy (STM)- Atomic Force Microscopy (AFM) principles.

Scanning tunneling microscopy (STM), an example of scanning probe microscopic techniques uses a sharp metal tip moving in a raster fashion to probe the local structure of surface of solid materials. During the last decade, Binnig and-coworkers [48] invented means of employing nanoscale processes such as electron tunneling and brought the resolution in the measurement virtually down to atomic scale. Further, using tiny cantilevers they demonstrated how forces between atoms could be exploited in obtaining topography of surfaces, a technique which is now known as Atomic Force Microscopy (AFM). These inventions would not have been possible without the advent of recent technology, which provided piezo scanners and associated electronics sensitive enough to measure nanoamps and nanomovements.

The underlying physical basis of the STM is electron tunneling [49,50]. Electron conducting occurs between two conductors separated by a sufficiently thin insulating layer or in physical terms, a tunneling barrier. In STM, when a metallic tip is advanced towards a sample, the tip and the sample wavefunctions start to overlap at very close distances. Upon application of a small bias voltage between the tip and the sample, a tunneling current will flow through the gap. The tunneling current depends critically on the wave function overlap. If this overlap is changed

either by changing tip-sample distance or by varying applied voltage, the tunneling will change with it.

If V is the bias voltage between tip (t) and the sample (s) the tunneling current between the two is given by

$$I = \int_0^{eV} \rho_s(r_s, E) \rho_t(r_t, \pm eV, \pm E) T(E, eV, r) dE \quad 1$$

Here ρ terms are density of states at energy E (relative to fermi energy) and at position r , The upper signs are for positive sample bias, and the lower signs are for negative sample bias. The tunneling transmission probability density T is given by

$$T(E, eV) = \exp \left[- \frac{2z(2m)^{1/2}}{\hbar} \left(\frac{\phi_s + \phi_t}{2} + \frac{eV}{2} - E \right)^{1/2} \right] \quad 2$$

and T depends exponentially on the sample-tip distance z and the square root of the sum of the work functions. This expression implies that the SPM image reveals local density of states at the fermi level (FLDOS) of the surface in the region being scanned which in general closely matches with the topography of the surface.

The AFM on the other hand, exploits forces, which exist between atoms and molecules [51]. In AFM, the force exerted upon a tip mounted

onto a cantilever with a known spring constant is monitored as the tip passes over the surface. The cantilever deflects during the scan and from the measurement of these deflections an image of the surface topography is obtained. All types of materials experience these forces and therefore the AFM, unlike the STM, is not limited to reasonable conductors.

There are two regimes of forces, which can be felt by the probing tip. If the tip is scanned extremely close to the surface of a sample, the force $F(r)$, will be expressed by

$$F(r) = 12 \frac{B}{r^{13}} - 6 \frac{D}{r^7} \quad 3$$

Where B and D are constants which depend upon specific properties of the atoms involved, such as the electron charge distribution between atoms of the tip and sample; r is the separation distances, the first term (the repulsive term) will dominate implying that the tip-atoms nearest to the sample surface will contribute almost all the information about its topography. While scanning at large separation distances, long-range attractive forces due to Van der Waals interaction dominate, which involve many-atom interactions between the tip and the sample. Therefore, when a cantilever-tip approaches a surface, its deflections will be the resultant of these factors and a force-distance curve related to the property of the tip and the surface may be obtained.

While the scanning is in progress, the computer and the servo loop in combination with a laser and a photodiode monitor the deflection of the cantilever which is proportional to the force exerted onto the cantilever-tip. Some important experimental parameters are the force F , usually a few nN; the spring constant K , the modulus of elasticity of the cantilever, usually between 1 and 100N/m; and the scan rate. There are three scanning modes for -AFM: Constant force, Constant Height and tapping. There is also two-force regime: contact or repulsive, non-contact or attractive. In the constant force regime, the tip is touching the sample surface where repulsive forces dominate and in non-contact regime, the tip is at a distance from the sample surface where the attractive forces dominate. Tapping mode is a compromise between these two - the cantilever is made to oscillate. This allows one to scan soft adsorbates on

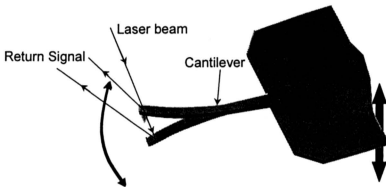


Figure 2.9 Schematic of the tapping cantilever in free air.

While the scanning is in progress, the computer and the servo loop in combination with a laser and a photodiode monitor the deflection of the cantilever which is proportional to the force exerted onto the cantilever-tip. Some important experimental parameters are the force F , usually a few nN; the spring constant K , the modulus of elasticity of the cantilever, usually between 1 and 100N/m; and the scan rate. There are three scanning modes for -AFM: Constant force, Constant Height and tapping. There is also two-force regime: contact or repulsive, non-contact or attractive. In the constant force regime, the tip is touching the sample surface where repulsive forces dominate and in non-contact regime, the tip is at a distance from the sample surface where the attractive forces dominate. Tapping mode is a compromise between these two - the cantilever is made to oscillate. This allows one to scan soft adsorbates on

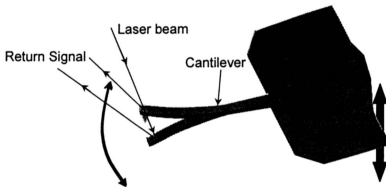


Figure 2.9 Schematic of the tapping cantilever in free air.

a substrate with better resolution and with less modification of the surface.

In this work Dimension 3000 SPM/AFM of Digital Instruments was used to collect the topographic information of the samples. As the interest is towards the topography rather than compositional analysis tapping mode method was used to scan the samples. Figure 2.9 represents a cantilever oscillating in free air at its resonance frequency. A piezo stack excites the cantilever's substrate vertically, causing the tip to bounce up and down. As the cantilever bounces vertically, the reflected laser beam is deflected in a regular pattern over the photo diode array, generating a

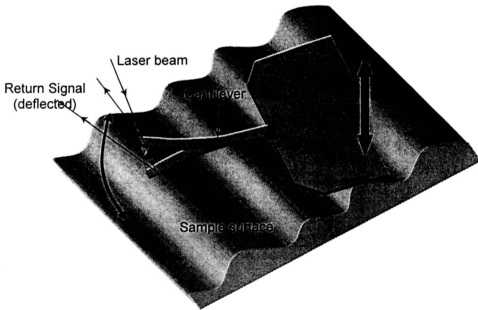


Figure 2.10 Schematic of the tapping cantilever on sample surface.

sinusoidal, electronic signal. Figure 2.10 represents the same cantilever oscillating over a sample surface, when the tip approaches the surface

the lever experiences a elastic bend due to the reasons discussed earlier and hence the return signal of the laser beam deviates from the previous one. When the tip scans the surface in a raster mode the differences in the return signal generates a sinusoidal electronic signal, which is used to reconstruct the image.

Though this technique is relative new, due to its various advantages discussed earlier it is becoming very popular, biologists have found this as an useful technique to study the enzymatic degradations of DNA [52]. A review by Hansma [53] covers the use of this technique in the field of Bio Molecular imaging. In the field of materials science also this technique is gaining importance, work done by Powell [55] and Neudeck [56] can be referred to as few examples in the field of Semiconductor technology. Electrodeposition is not left untouched by this technique, it has been widely used to study the nucleation of various metals and alloys, Amster [57] has used this technique to study the nucleation of copper deposition on palladium. Morphological evaluations, done by Kondo et.al. [58] on zinc electrodeposits and the research done by Kiyokawa et.al. [59] are few classical examples of the application of AFM in the field of electrodeposition.

2.3.5 Electrochemical impedance

Of all the electrochemical tests, the simplest to perform is the corrosion measurement of corrosion potential as a function of immersion time but its results are difficult to interpret. The electrochemical resistance of the coating could give an indication of its efficiency as a barrier to ions [60]. Other electrochemical methods like electrochemical resistance measurement, anodic and cathodic polarization studies, either need a lot of corrections to meet over the potential drops due to the internal ohmic resistance, or they are not a non-destructive method [61]. For example anodic or cathodic polarization method can not be used in studying the corrosion protection properties of a paint system, as they intend to change the conditions at the metal/paint interface layer so that the technique itself may cause defects in the coating [62].

Since many coatings are intended to provide corrosion protection over extended periods, it is highly useful to set lifetime specifications. Thus, typical coating tests can take hundreds or thousands of hours. The result of such tests has been correlated with varying degree of success, to actual in-service performances. Factors such as rapidly changing technology, environmental conditions, and the time constraints, often make it difficult to perform long-term evaluations. It is also difficult to perform in-service tests on large engineering structures, such as bridges, or costly production items. Thus improved methods for characterizing

coating system's performance are continuously sought and developed. A large number of methods are available for evaluation of coating systems. Many of the standard test for coatings relate to material specifications, mechanical properties, or appearance. Others such as salt spray test, provide accelerated performance testing [63]. There are few electrochemical and electrical methods available to determine the performance of a coating, they are DC electrical properties, electrochemical impedance, capacitance, corrosion potential, and polarization curves, polarization resistance, potentiodynamic polarization curves, cathodic delamination and other methods. Electrochemical impedance method is becoming a powerful tool in the study of corrosion [64], semiconductors [65], batteries [66], electroplating [67] and electro-organic synthesis [68]. Electrochemical impedance technique offers three major advantages over other DC techniques:

- Small amplitude
- Mechanism study
- Accuracy

The main advantage of EIS* is that one can use a purely electronic model to represent to represent an electrochemical cell. An electrode interface undergoing an electrochemical reaction is typically analogous to an electronic system consisting of a specific combination of resistors and capacitors. In practice the data obtained from a given electrochemical

*EIS – Electrochemical Impedance Spectroscopy

system can be used to correlate with one or more equivalent circuits, or at least it can be used to eliminate the incorrect models. Once the model is chosen then it can be used to correlate the physical and chemical properties with circuit elements and extract numerical values by fitting the data to the circuit model.

2.3.5.1 Theory

The term resistance in a DC circuits denoted the opposition to the flow of electrons or *current*, in DC circuits resistance is the only element which produces this effect. Whereas in an AC circuit the opposition to the flow is called as impedance and it is not a single element, but is usually a combination of two other circuit elements capacitance and inductance. Impedance can be expressed as a complex number, where the resistance is the real component and the capacitance or the inductance is the imaginary component. This special treatment for the opposition of the electron in an AC circuit is because of the phase shift experienced by the current wave. In Figure 2.11 E is the voltage sine wave applied across the circuit I is the current waveform, it should be noted that the I wave form is different from the input signal E waveform. The current sine wave can be described by the equation [68]:

$$I(t) = A \sin(\omega t + \theta)$$

$I(t)$ = Instantaneous current
 A = maximum amplitude

ω = frequency in radians per second = $2\pi f$ (f = frequency in Hertz)
 t = time
 θ = phase shift in radians

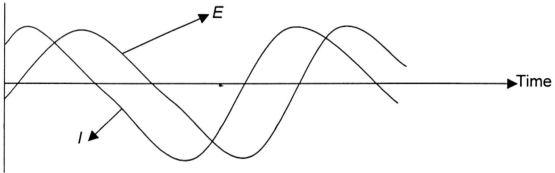


Figure 2.11 Typical voltage sine wave (E) applied across a circuit and the resultant current wave form (I)

Using the complex number convention, an AC current vector can be split into two components namely real and imaginary components where Imaginary part is a complex number I . These real and imaginary components are defined with respect to some reference waveform. The real component is in phase with the reference waveform and the imaginary component is exactly 90 degrees out of phase.

$$I_{\text{total}} = I' + I'' j \quad (1)$$

Where

$$j = \sqrt{-1}$$

I' = real component

I'' = Imaginary component

ω = frequency in radians per second = $2\pi f$ f =frequency in Hertz)

t = time

θ = phase shift in radians

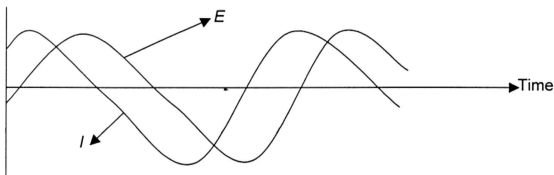


Figure 2.11 Typical voltage sine wave (E) applied across a circuit and the resultant current wave form (I)

Using the complex number convention, an AC current vector can be split into two components namely real and imaginary components where Imaginary part is a complex number I . These real and imaginary components are defined with respect to some reference waveform. The real component is in phase with the reference waveform and the imaginary component is exactly 90 degrees out of phase.

$$I_{\text{total}} = I' + I'' j \quad (1)$$

Where

$$j = \sqrt{-1}$$

I' = real component

I'' = Imaginary component

In DC theory (an AC current where frequency of the input wave form is zero) the resistance offered to the electron flow is given by Ohm's law as:

$$E = IR \quad (2)$$

Where
E = Applied Potential
I = Current
R = Resistance

When the frequency is not zero i.e. the current is AC then the analogous equation is

$$E = IZ \quad (3)$$

Where

E = Applied Potential
I = Current
Z = Impedance

The voltage vector E can also be resolved into real and imaginary components like current and hence

$$E_{total} = E' + E'' j \quad (4)$$

substituting equations 1 and 4 in 3, Z can be expressed as

$$Z_{total} = \frac{E' + E'' j}{I' + I'' j} \quad (5)$$

where

$$Z_{total} = Z' + Z'' j \quad (6)$$


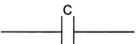
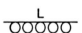
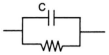
the absolute of the total impedance Z_{total} can be expressed as

$$|Z| = \sqrt{Z'^2 + Z''^2} \text{ and the phase angle can be defined by equation (7)}$$

$$\tan \theta = \frac{Z''}{Z'} \quad (7)$$

the following Table 2.1 shows the various circuit elements and their impedance equation.

Table 2.1 Various Circuits elements and their impedance equations.

Circuit Elements	Impedance Equation
 R	$Z = R + 0j$ $j = \sqrt{-1}$
 C	$Z = 0 - \frac{j}{\omega C}$ $\omega = 2\pi f$
 L	$Z = 0 + j\omega L$ $\omega = 2\pi f$
	$Z = \frac{R}{1 + \omega^2 C^2 R^2} - \frac{j\omega C R^2}{1 + \omega^2 C^2 R^2}$

R = Resistor; C = Capacitor; L = Inductor

Variety of formats were available to analyze the impedance data viz., Nyquist or Cole-Cole plot (real and imaginary components of the impedance were plotted), Bode plot ($\log f$ versus $\log |Z|$ as well as θ versus $\log f$), Randles plot ($\sqrt{\omega}$ vs. Z'). Even though every format has its own and unique advantages, Nyquist or Cole-Cole plot is the most popular, primary reason is due to the ease in seeing the effects of the ohmic resistance.

2.3.5.2 Nyquist or Cole-Cole plot

Figure 2.12 shows the Cole-Cole plot of the impedance data, where the real component of the impedance is plotted on the abscissa and the negative of the imaginary component is plotted on the ordinate

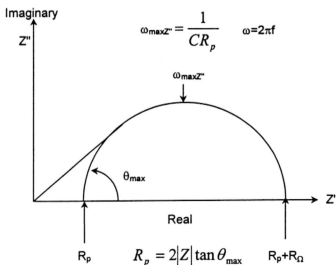


Figure 2.12 Nyquist or Cole-Cole plot for a simple electrochemical system

axis at each excitation frequency. The frequency reaches its high limit at the left most end of the semicircle, where the semicircle touches the x-axis and the frequency reaches its low limit at the right most end of the semicircle. The value at which the high frequency data meets the x-axis is the polarization resistance (R_p). The value at which the low frequency data meets the x-axis is sum of the ohmic resistance and polarization

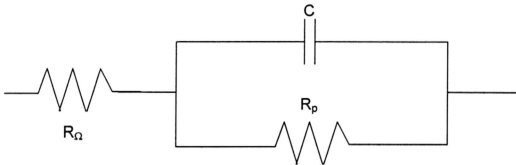


Figure 2.13 Equivalent circuit for the Cole-Cole plot shown in figure 2.12
 R_p = Polarization resistance
 C = Capacitor
 R_{Ω} = Solution resistance

resistance ($R_p + R_{\Omega}$). Typical equivalent circuit for the plot mentioned above in figure 2.12 would be as shown in figure 2.13.

Electrochemical impedance spectroscopy has found a wide spread application due to the quantum of information, which can be obtained. The field of application ranges from semiconductors to paint coatings. A series of literatures published by Westing et.al. [69-75] covers

the wide range of application of this technique in determination of the protective coatings performance. Elsener [76] group used this technique to study the corrosion of PVD and CVD titanium nitride coatings. Passive films on AISI 304 stainless steel were studied by Simoes et.al.[77]. In the present study this technique is being used to study the barrier coatings obtained by spray pyrolysis.

The impedance values at various frequencies are measured using HIOKI 3520 LCR HI TESTER. The impedance value (Z) was resolved into imaginary and real component using the following equations

Real part of impedance

$$Z' = Z \cos \theta$$

Imaginary part of impedance

$$Z'' = -Z \sin \theta$$

Where θ is the phase shift, measured by the instrument. A time interval of 10 seconds was given between two successive readings. The imaginary and real parts were then plotted to obtain the Cole-Cole plot. Figure 2.14 shows the experimental setup for impedance measurement done in this study.

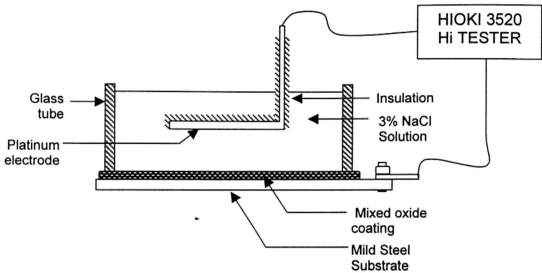


Figure 2.14 Schematic of the experimental setup used in this study to collect impedance data.

2.3.6 Open Circuit Potential Measurement

Baldwin et.al. [85] used the open circuit potential (OCP) study on their zinc-nickel alloy and concluded that the alloy became electrochemically less active as the concentration of the more noble metal increases. Though this method is a crude one and does not give any information about the mechanism followed during the process of corrosion, it is still possible to determine whether the coating behaves sacrificially to the mild steel substrate or not. OCP measurement was done on both the zinc-nickel codeposit and zinc-cobalt codeposit. Mainly this test was done to evaluate the difference in behavior of the air-agitated deposits and the sonicated deposits. Figure 2.15 shows the experimental setup used for this OCP measurement. The potentials were

measured using a Ag/AgCl electrode. The samples were covered with epoxy resin leaving a surface area of 1cm^2 , electrical connections to the sample and the potential measuring device using a riveted copper wire which also enclosed by epoxy resin to minimize the establishment of galvanic coupling between the current collector and the samples. Then the samples are immersed in 3% NaCl solution, after one hour of immersion the potential was measured using a KEITHLEY 195 Digital

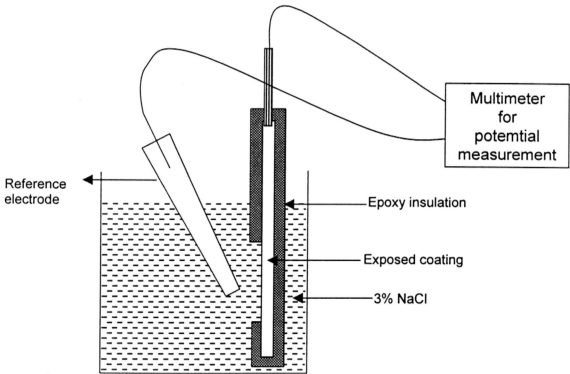


Figure 2.15 Schematic of experimental setup used for OCP measurement.

Multimeter. During the potential measurement the reference electrode was placed as close as possible to the surface of the coating. Potentials

are then measured at stipulated time intervals and the measured potentials were plotted against time.

Following chapters III, IV, V, is the results and discussions of the experimental studies done on the zinc-nickel alloy deposition, zinc-cobalt alloy deposition and multi element metal oxide coating respectively.